

Supplementary Information

A flexible back-contact perovskite solar micro-module

Michael Wong-Stringer^{1,α}, Thomas J. Routledge^{1,α}, Trevor McArdle², Christopher J. Wood², Onkar S. Game¹, Joel A. Smith¹, James E. Bishop¹, Naoum Vaenas¹, David M. Coles^{1,3}, Alastair R. Buckley^{1,3} and David G. Lidzey^{1,3*}

¹Department of Physics & Astronomy, University of Sheffield, Hicks Building, Hounsfield Road, Sheffield, S3 7RH, United Kingdom

²Power Roll Limited, Washington Business Centre, 2 Turbine Way, Sunderland, SR5 3NZ, United Kingdom

³Ossila Limited, Windsor Street, Sheffield, S4 7WB, United Kingdom

^αThese authors contributed equally to this work

*Corresponding author, email d.g.lidzey@sheffield.ac.uk

Keywords: perovskite solar module, flexible, back contact, rare-metal free, groove, electron-beam evaporation, scalable, low-temperature.

Supplementary Figures & Tables

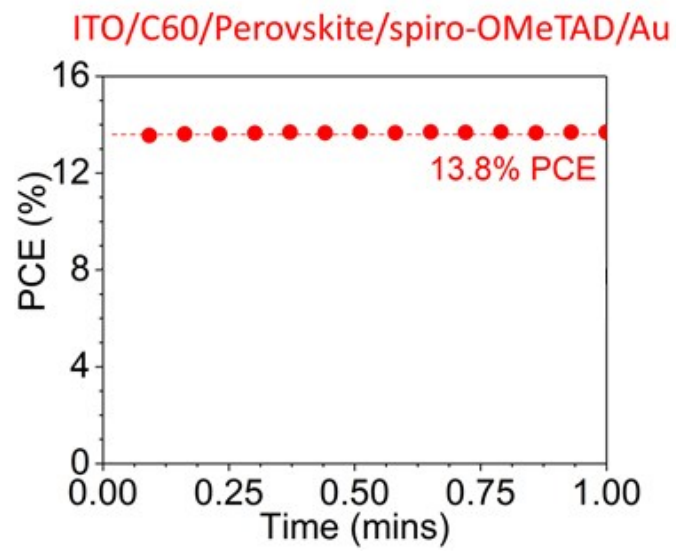


Figure S1: Stabilised power conversion efficiency output of flat standard architecture ITO/C₆₀/MAPbI₃/spiro-OMeTAD/Au PSC.

Simulated 2D Photocurrent Generation

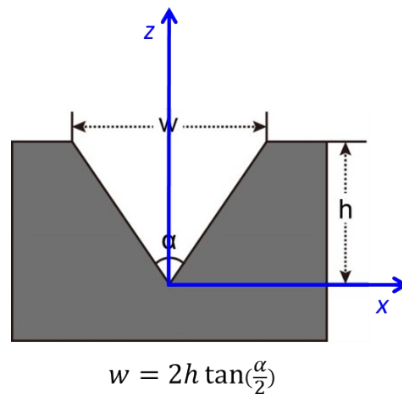


Figure S2: Cross-sectional view of a typical groove with width 'w' and angle 'alpha'.

A simplified 2D model was developed on the basis of charge carrier generation and collection probabilities, and was used to simulate photocurrent generation within a groove device. For electron-hole (e-h) pairs generated within the groove, the probability of collection at the respective electrodes is assumed to be limited by the minority carrier diffusion length L_d (holes in the case of $\text{CH}_3\text{NH}_3\text{PbI}_3$). The charge carrier collection probability for a perovskite filled 2D groove device can therefore be represented as;

$$C(\theta, z) = e^{-\left(\frac{z \tan(\theta) + z \tan\left(\frac{\alpha}{2}\right)}{L_d}\right)}$$

where the geometrical distances are those shown in Figure S2. The photo-carrier generation within groove dimensions is assumed to be limited by the absorption coefficient of perovskite composition according to the Beer-Lambert law as;

$$P(z) = P_0 e^{-\left(\frac{h-z}{D}\right)}$$

where, D is the light penetration depth at a particular wavelength calculated from the absorption coefficient. The photo-generated current through this 2D groove model can then be written as;

$$I(h, \alpha) = \left(\int_{-\alpha/2}^{\alpha/2} d\theta \int_0^h dz P(z) C(\theta, z) \right) / V_{oc}$$

Using this expression, the photocurrent variation within the width of groove can be estimated using material specific parameters D and L_d . For a symmetric groove ($\alpha = 60^\circ$), filled with $\text{CH}_3\text{NH}_3\text{PbI}_3$ (D near band edge ≈ 800 nm and $L_d \approx 500$ nm), we find the

optimum groove width necessary to maximize photo-current to be $\approx 1.1 \mu\text{m}$ (see Figure S3a).

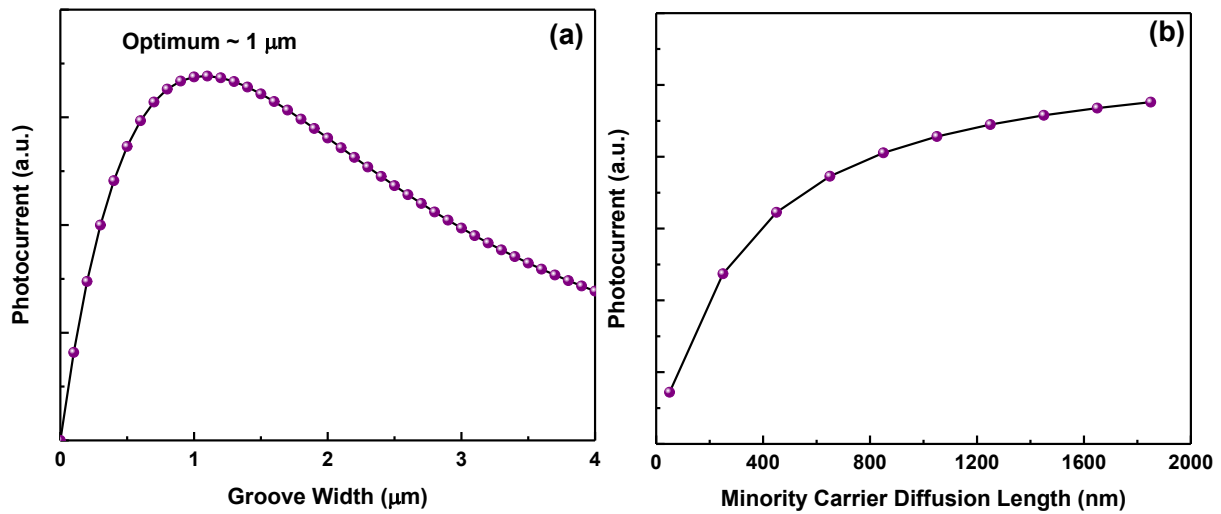


Figure S3: Variation of photocurrent generated by groove as a function of (a) groove width and (b) hybrid-perovskite minority carrier diffusion length.

The results obtained from this simplified 2D model are supported by our experimental measurements on single groove devices with different widths as shown in Figure 2(c) and Table 1. Here, we observed higher efficiency with a groove width of $1.6 \mu\text{m}$ (PCE = 7.03%) than $3 \mu\text{m}$ (PCE = 4.83%). With more control over microfabrication techniques we aim to reduce the groove width to the optimum value of $1.1 \mu\text{m}$.

Our simulations indicate that the minority carrier diffusion length (L_d) of perovskite also directly influences the power conversion efficiency. Figure S3b shows a monotonic increase in photocurrent with L_d up to 1600 nm ; a result that suggests that perovskite composition along with grain size will have a significant impact on the performance of groove-based cells.

Further evidence for the importance minority carrier diffusion length can be seen in Figure S4a and S4b. Here, we plot the spatial distribution of the generated photocurrent for two different carrier diffusion lengths. Here, if we assume electrons to be minority carriers with an L_d of 200 nm , we find that only regions very close to the ETL interface contribute to photocurrent. In contrast for an L_d of 500 nm , most of the material within the groove contributes to the photocurrent.

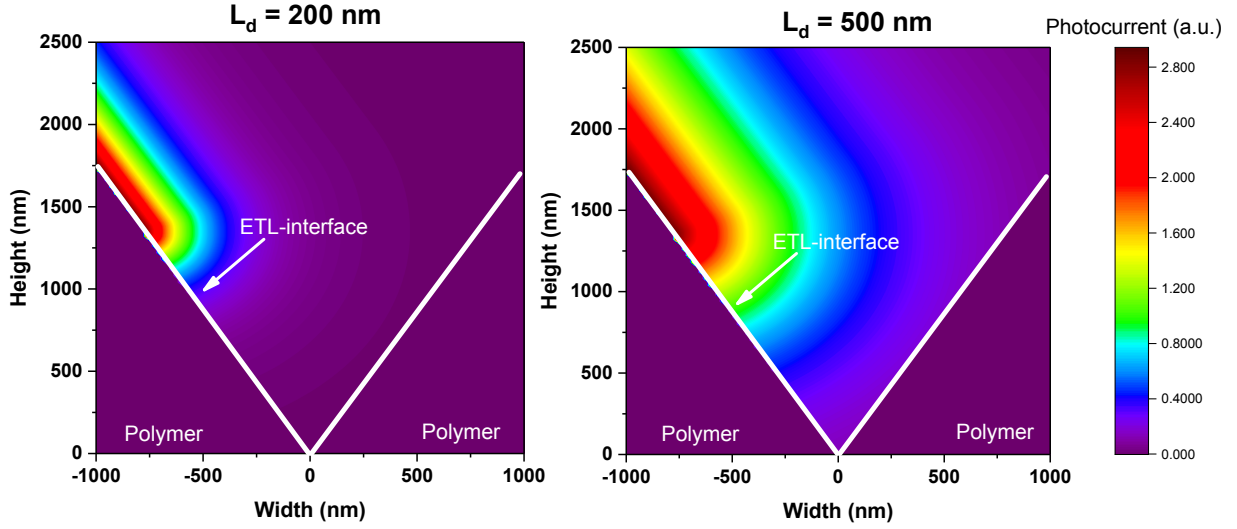


Figure S4: Spatial contribution of the photocurrent from a perovskite within the groove having a minority carrier diffusion length L_d of (a) 200 nm and (b) 500 nm

In order to obtain further insight into the electronic characteristics of groove devices we fitted the JV curves of single groove devices to the single diode model of a solar cell as given by;

$$J = J_0 \left[e^{\left(\frac{V - JR_s}{nV_t} \right)} - 1 \right] + \frac{V - JR_s}{R_{sh}} - J_{ph}$$

where $V_t = \frac{k_B T}{q}$, n is diode ideality factor, J_0 and J_{ph} correspond to reverse saturation current density and photocurrent density respectively and R_s and R_{sh} denote the series and shunt resistance respectively. Figure S5 shows JV fits to a 1-diode model for single 1.6 μm and 3 μm width grooves having a high diode ideality factor (~ 5) and a reverse saturation current density of $\sim 6.1 \mu\text{A}/\text{cm}^2$. Diode ideality factors greater than 2 have been associated with nonlinear shunt pathways near mechanical defects such as scratches and edges which can act as source of leakage current.¹ Whilst the series resistance for 1.6 μm groove ($\sim 12 \Omega \cdot \text{cm}^2$) and 3 μm groove ($\sim 15 \Omega \cdot \text{cm}^2$) were of similar order of magnitude, the shunt resistance of the 1.6 μm groove device ($\sim 60 \Omega \cdot \text{cm}^2$) is considerably smaller than 3 μm groove device ($\sim 395 \Omega \cdot \text{cm}^2$).

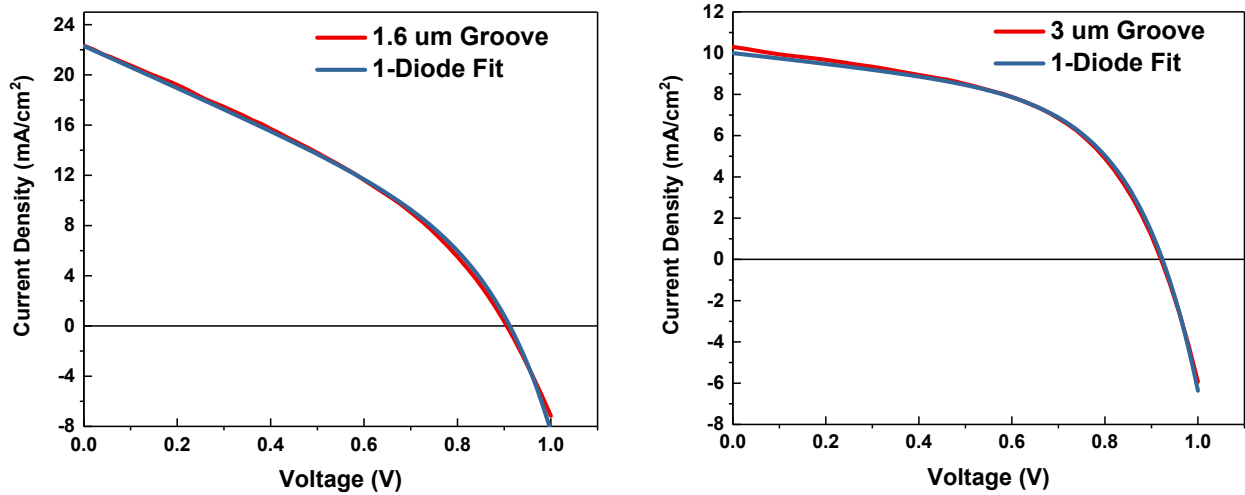


Figure S5: *JV curves of single groove devices fitted to 1-diode model.*

We note that other considerations such as recombination dynamics at the grain boundaries, electrode interfaces and resistive losses due to presence of voids during perovskite deposition can affect the overall efficiency and hence the optimum geometry. However, the simplified model described above gives a reasonably good starting point to design grooves to maximize the power conversion efficiency.

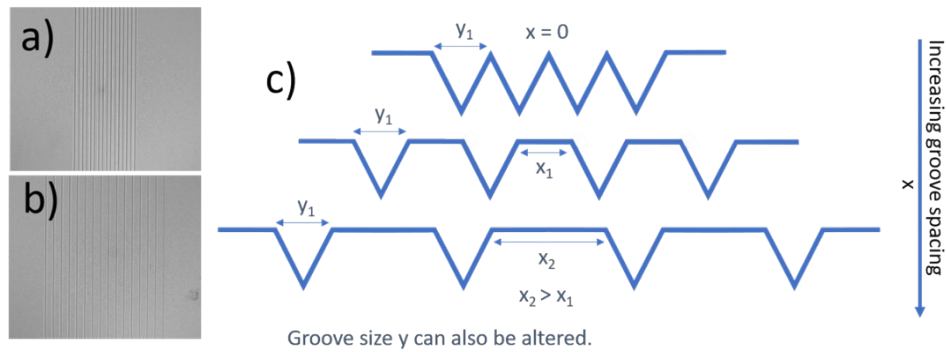


Figure S6: Top down focussed ion beam-scanning electron microscopy images a) and b) showing a groove spacing of $0.5\ \mu\text{m}$ and $3\ \mu\text{m}$ respectively. c) A simple diagram indicating how the groove size and spacing can be altered.

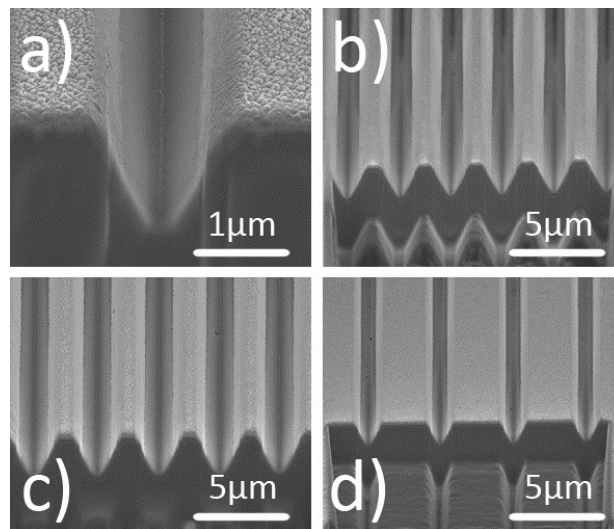


Figure S7: Focussed ion beam-scanning electron microscopy images of grooves before perovskite deposition. a) A $1.6\ \mu\text{m}$ wide single groove. b) A multi-groove pattern with $2\ \mu\text{m}$ grooves and $0.5\ \mu\text{m}$ spacing. c) A multi-groove pattern with $3\ \mu\text{m}$ grooves and $0.5\ \mu\text{m}$ spacing. d) A multi-groove pattern with $2\ \mu\text{m}$ grooves and $3\ \mu\text{m}$ spacing.

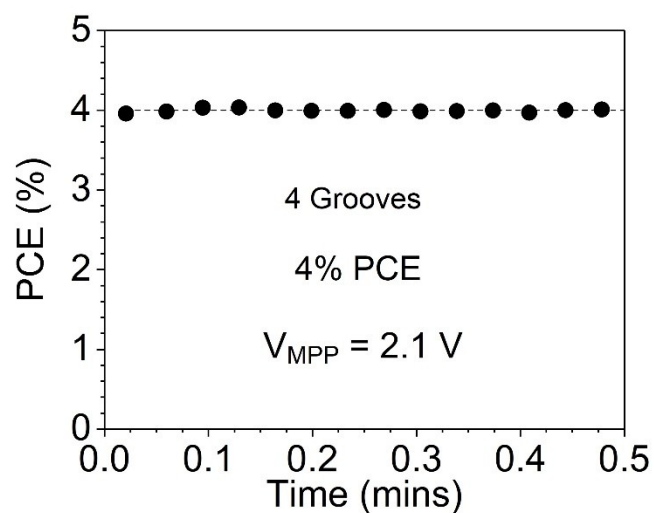


Figure S8: Stabilised power conversion efficiency output of the champion four groove solar micro-module presented in Figure 3.

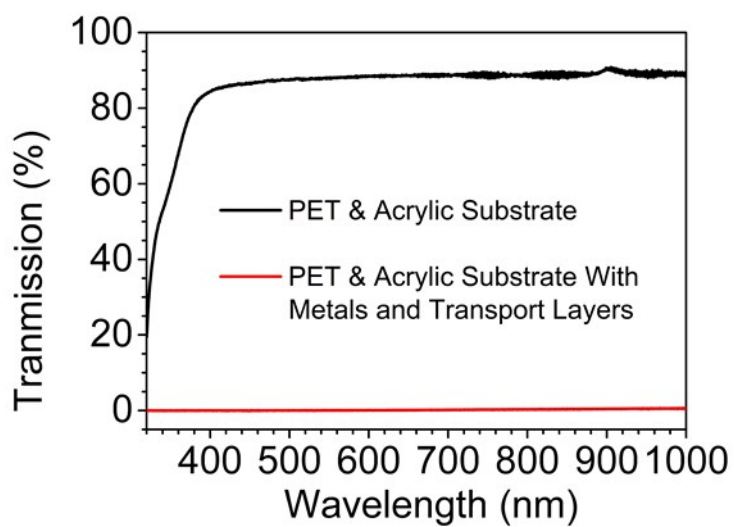


Figure S9: UV-Visible transmission spectra of the PET:acrylic substrate before (black) and after (red) the deposition of the metal electrodes and transport layers.

Groove Width Used for Active Area	Groove Width [μm]	Illumination Mask?	Stabilised PCE [%]
Groove Width	2	Not Possible	4
Back Illumination	1	Yes (Self Masking)	4.4

Table S1: Stabilised power conversion efficiencies obtained when using: standard front illumination, where the groove width is used to calculate the active area, and back illumination, where the thick metal electrodes are used as an integrated illumination mask. Width of groove and masked width are checked with focussed ion beam-scanning electron microscopy.

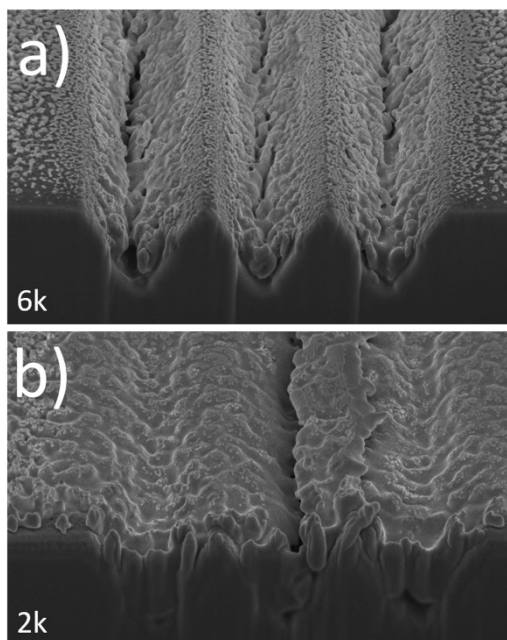


Figure S10: Focussed ion beam-scanning electron microscopy images of multi-grooves after different MAPbI_3 spin coating solution depositions. a) Spin speed of 6000 rpm. b) Spin speed of 2000 rpm.

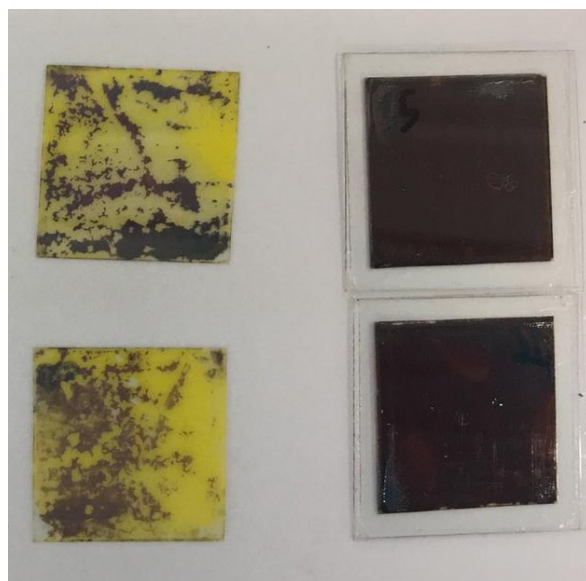


Figure S11: Preliminary encapsulation strategies for PSC grooves. Here PET:acrylic substrates were coated with MAPbI_3 and left unencapsulated or sealed with 3M UBF-512 barrier films with Adhesive Research pressure sensitive adhesive (PSA). This picture shows such films after they have been stored at 80 % RH for 3 weeks without encapsulation (on the left) and with encapsulation (on the right).

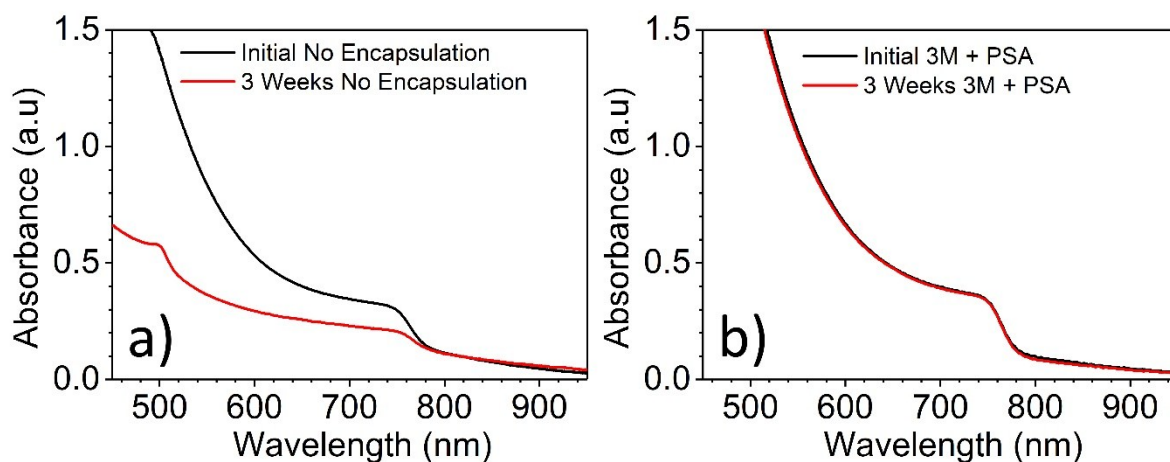


Figure S12: UV-visible transmission spectra of the PET:acrylic substrate coated with MAPbI_3 before (black) and after (red) such films have been stored at 80 % RH for 3 weeks with either a) no encapsulation, or b) sealed as described in Figure S11.

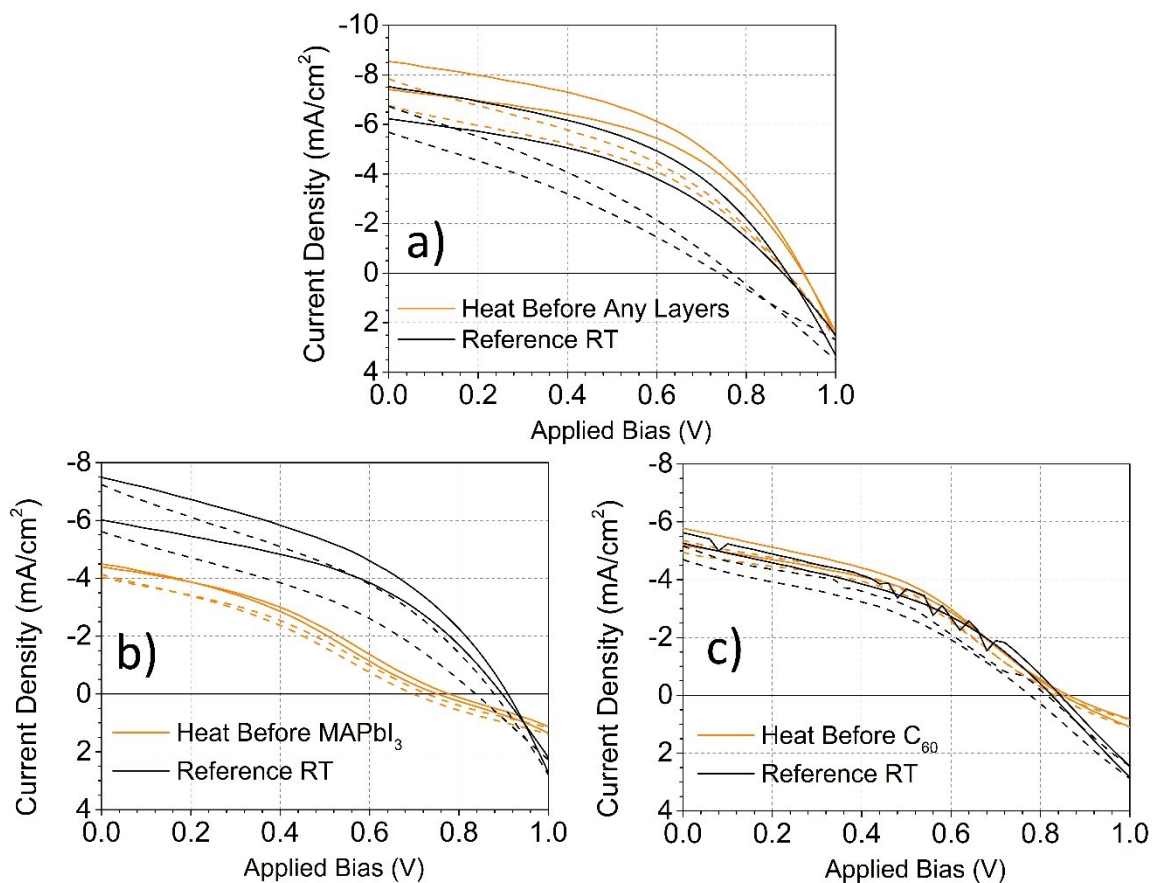


Figure S13: Current-voltage curves of characteristic $3.7 \mu\text{m}$ wide single grooves left untreated (red) or heat treated (black) for 1 hour at 110°C in air either, a) before any materials were deposited onto the grooves, b) before the MAPbI_3 was deposited, or c) before the C_{60} was deposited (with all other electrode materials present). Solid and dotted lines represent reverse and forward sweeps respectively. Reference untreated PSC grooves were fabricated for every set of measurements to account for batch-to-batch performance variations. Devices did not have an Al_2O_3 layer below the electrodes and had a directionally coated nickel base layer positioned below the titanium electrode to improve substrate conductivity.

Table S2: *Solar cell performance metrics of the PSC solar groove micro-modules as described and shown in Figure S12.*

References

- 1 O. Breitenstein, P. Altermatt, K. Ramspeck, A. Schenk, *Proceedings of the 21st European Photovoltaic Solar Energy Conference, 2006*, **21**.